J. Fluid Mech. (2011), *vol.* 670, *pp.* 581–605. © Cambridge University Press 2011
doi:10.1017/S0022112010005616

A dynamic multi-scale approach for turbulent inflow boundary conditions in spatially developing flows

GUILLERMO ARAYA[1]†, LUCIANO CASTILLO[2], CHARLES MENEVEAU[1] AND KENNETH JANSEN[2]

[1]Department of Mechanical Engineering, Johns Hopkins University, Baltimore, MD 21218, USA

[2]Department of Mechanical, Aeronautical and Nuclear Engineering, Rensselaer Polytechnic Institute, Troy, NY 12180, USA

(Received 18 December 2009; revised 14 October 2010; accepted 21 October 2010)

A dynamic method for prescribing realistic inflow boundary conditions is presented for simulations of spatially developing turbulent boundary layers. The approach is based on the rescaling–recycling method proposed by Lund, Wu & Squires (*J. Comput. Phys*, vol. 140, 1998, pp. 233–258) and the multi-scale method developed by Araya, Jansen & Castillo (*J. Turbul.*, vol. 10, no. 36, 2009, pp. 1–33). The rescaling process requires prior knowledge about how the velocity and length scales are related between the inlet and recycle stations. Here a dynamic approach is proposed in which such information is deduced dynamically by involving an additional plane, the so-called test plane located between the inlet and recycle stations. The approach distinguishes between the inner and outer regions of the boundary layer and enables the use of multiple velocity scales. This flexibility allows applications to boundary layer flows with pressure gradients and avoids the need to prescribe empirically the friction velocity and other flow parameters at the inlet of the domain. The dynamic method is tested in direct numerical simulations of zero, favourable and adverse pressure gradient flows. The dynamically obtained scaling exponents for the downstream evolution of boundary layer parameters are found to fluctuate in time, but on average they agree with the expected values for zero, favourable and adverse pressure gradient flows. Comparisons of the results with data from experiments, and from other direct numerical simulations that use much longer computational domains to capture laminar-to-turbulence transition, demonstrate the suitability of the proposed dynamic method.

Key words: turbulent boundary layers, turbulence modelling, turbulence simulation

1. Introduction

While computational fluid dynamics has gone through notable developments in the last few decades, spatially developing turbulent flows such as boundary layers near walls are still very challenging to be computed numerically because of the difficulties associated with the prescription of inflow boundary conditions. The most

† Email address for correspondence: araya@mailaps.org

straightforward approach consists of starting from the easy-to-specify laminar regime including disturbances and simulating transition to turbulence and, finally, using this information as input to the main domain of interest (Rai & Moin 1993; Skote 2001; Khujadze & Oberlack 2004; Schlatter *et al.* 2009; Wu & Moin 2009). Resolving the transition in simulations of developing flows has the advantage that there is no need to prescribe realistic turbulent fluctuations at the inlet. However, the main drawback is the high computational cost due to the need for very long computational domains and the ensuing limitations regarding the highest achievable Reynolds number. On the other hand, several techniques for modelling turbulent inflow conditions have been put in practice, with different degrees of success. A comprehensive review can be found in Lund *et al.* (1998) and Moin & Mahesh (1998) and more recently in Keating *et al.* (2004).

The simplest approach is to superimpose random fluctuations on a desired mean profile. The random fluctuation method has been applied with different variants (e.g. Lee *et al.* 1992; Le & Moin 1994; Park & Choi 1999). Unfortunately, the use of random fluctuations requires long developing regions to obtain physically realistic flow structures. To overcome some of these drawbacks, Klein, Sadiki & Janicka (2002) utilized digital filters to generate velocity profiles from random noise. Because the filtering technique was restricted to equidistant grid-spacing meshes, Kempf, Klein & Janicka (2005) presented a more general method to artificially generate initial and inflow conditions, based on a diffusion process that transformed white noise into a signal by prescribing integral length scales and Reynolds stress tensors.

In an important development, Lund *et al.* (1998) proposed a modification to the approach of Spalart & Leonard (1985) to account for the spatial growth, based on similarity laws of the velocity profiles at different locations in a spatially developing zero pressure gradient (ZPG) turbulent boundary layer. They considered an auxiliary simulation in which the velocity field was extracted from a downstream plane, the 'recycle plane'. The field was rescaled and reintroduced as a boundary condition at the inlet of the auxiliary zone. Subsequently, the instantaneous velocity field on a selected plane of the auxiliary domain was utilized as inflow information for the principal domain. However, the technique is limited in principle to ZPG equilibrium boundary layers. The limitation arises because of the assumption of a single velocity scaling for the inner and outer regions and the need to prescribe empirical correlations that connect the friction velocities u_τ between the inlet and recycle planes. A variant of the Lund approach was introduced by Ferrante & Elghobashi (2004, 2005) by imposing an appropriate energy spectrum for the turbulence kinetic energy and a condition to ensure a non-vanishing value of the shear Reynolds stresses at the inlet plane. Ferrante & Elghobashi (2005) performed direct simulations over a flat plate at momentum thickness Reynolds numbers up to 2900.

As a consequence of these and other challenges, simulations of spatially developing turbulent boundary layers with pressure gradients are still relatively scarce. The first direct numerical simulations (DNS) of boundary layers under pressure gradients were conducted by Spalart & Leonard (1985) and Spalart (1986). Periodic boundary conditions were imposed along the streamwise direction by including small growth terms in the governing equations. The growth-term approach produced satisfactory results in ZPG (Spalart 1988) and favourable pressure gradient (FPG; Spalart 1986) flows, but it was less successful in adverse pressure gradient (APG) flows because the assumption of slight streamwise inhomogeneity was not satisfied. Na & Moin (1998) carried out direct simulations of two spatially developing turbulent boundary layers under mild and strong APGs, with induced separation for the latter case. The

turbulent inflow conditions were generated from the DNS data of Spalart (1988) for ZPG turbulent boundary layers, the principal purpose of this investigation being the analysis of space–time characteristics of wall-pressure fluctuations in APG flows. Skote (2001) performed a series of DNS in self-similar turbulent flows, ranging from ZPG to APG flows, by resolving the full laminar-to-turbulence transition. He used a spectral code with streamwise periodicity and furthermore used the 'fringe' method to damp the turbulence back to the desired laminar inflow profile. Later, Lee & Sung (2008) performed direct simulations of equilibrium APG flows by prescribing a power-law free-stream velocity $U_\infty \sim x^m$, as in Skote (2001). To avoid the computation of the laminar–transition stage, they prescribed the turbulent inflow conditions based on the method of Lund *et al.* (1998), considering a ZPG zone prior to the APG region, but this still required a very long computational domain to allow for the required adjustments in the flow. Xu and Martin (2004) proposed an inflow generation technique for spatially-evolving turbulent boundary layers in compressible flows, based on the rescaling-recycling method of Lund *et al.* (1998). Xu and Martin (2004) showed results for a supersonic turbulent flat plate (the streamwise length was roughly six inlet boundary layer thicknesses) at zero pressure gradient, obtaining good agreement with the theory. More recently, Simens *et al.* (2009) simulated boundary layers with and without pressure gradients. For ZPG cases, they used the approach of Lund *et al.* (1998) to generate the turbulent inflow conditions, where the momentum thickness Reynolds numbers spanned the range 620–2140. Furthermore, they simulated a strong-APG case with separation by assuming a laminar flow at the inflow to be triggered to the turbulent regime downstream, which resulted in a very long required computational domain of approximately 173 inlet boundary layer thicknesses.

The objective of this paper is to introduce a methodology that enables us to prescribe inlet turbulent conditions for a general class of boundary layer flows including those subject to pressure gradients. The methodology addresses the two limitations of the original rescaling–recycling approach (Lund *et al.* 1998) mentioned above: (i) the dependency on empirical correlations for downstream development is addressed using a dynamic approach in which the development of the simulated flow is interrogated to determine the required parameters; and (ii) the limitation of using single velocity scales across different layers is generalized with a multi-scale procedure that may better absorb the pressure gradient effects. A non-dynamic version of this multi-scale approach has recently been described in Araya (2008) and Araya *et al.* (2009). The new approach is tested in a suite of DNS of boundary layers with different pressure gradients and Reynolds numbers, and results are compared with experimental data, as well as with results from costlier DNS without a recycling method that must use much longer computational domains to capture transition.

2. The dynamic multi-scale rescaling–recycling method

We concern ourselves with simulating a boundary layer as shown in the schematic in figure 1. Turbulent inflow boundary conditions are needed at the inlet plane at x_{inl}. The Cartesian coordinates x, y and z denote the streamwise, wall-normal and spanwise directions, respectively. The flow is divided into inner and outer regions (further generalizations including free-stream turbulence would require a third, free-stream, region). Also, the instantaneous velocity u_i is decomposed into a mean value U_i and a fluctuation u_i'. The basic idea of the rescaling–recycling method of Lund *et al.* (1998) is to construct a time-dependent velocity field at the inlet separately in

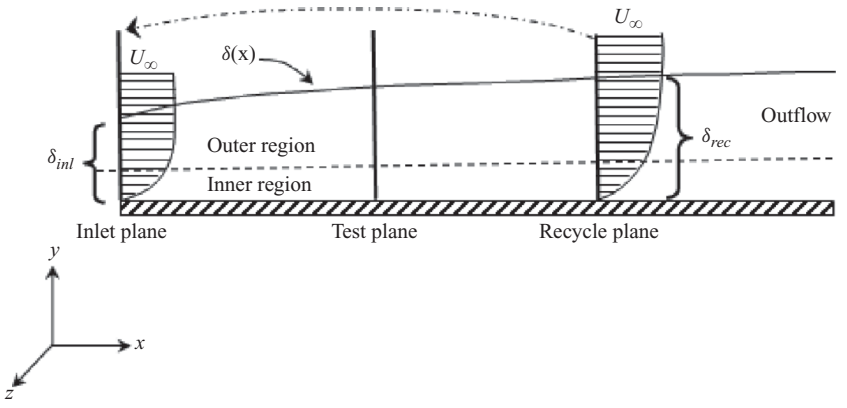

FIGURE 1. Schematic of the evolving boundary layer, with the inlet, recycle and test planes.

the inner (superscript (i)) and outer (superscript (o)) regions, according to

$$u_i(x_{inl}, y, z, t) = \left[(U_i)^{(i)}_{inl} + (u'_i)^{(i)}_{inl}\right]\{1 - W(\eta)\} + \left[(U_i)^{(o)}_{inl} + (u'_i)^{(o)}_{inl}\right]W(\eta), \tag{2.1}$$

where $\eta = y/\delta$ and $\delta(x)$ is the boundary layer thickness. The function $W(\eta)$ is a weighting function that goes smoothly from 0 near the wall in the inner region (small $\eta = y/\delta$) to $W(\eta) \to 1$ in the outer region ($\eta \to 1$). For $W(\eta)$ we use the same tanh profile of Lund *et al.* (1998), namely $W(\eta) = 0.5\{1 + \tanh[\alpha(\eta - b)/((1 - 2b)\eta + b)]/\tanh(\alpha)\}$, where $\alpha = 4$ and $b = 0.2$. Thus the mean and fluctuating velocities can be specified on the basis of the mean and fluctuating velocities at the recycle plane, but separately for the inner and outer regions. In the inner region, the fluctuating velocities are rescaled by matching the inner height in wall units above the wall between the recycle and inlet planes and by rescaling the velocities through the friction velocity scale. For example, the fluctuating velocity in the inner region, $(u'_i)^{(i)}_{inl} \equiv u'^{(i)}_i(x_{inl}, y, z, t)$, at some height y is obtained from the corresponding height at the recycle plane according to

$$u'^{(i)}_i(x_{inl}, y, z, t) = \lambda^{(i)}_{u'}\, u'_i\left(x_{rec}, \lambda^{(i)}_{u'} y, z, t\right), \tag{2.2}$$

where

$$\lambda^{(i)}_{u'} = \frac{(u_\tau)_{inl}}{(u_\tau)_{rec}} \tag{2.3}$$

is the scaling factor appropriate for all the fluctuating velocities at the inlet and recycle planes, in the inner region. Here, $u_\tau = \sqrt{\tau_w/\rho}$ is the local friction velocity; τ_w is the wall shear stress; and ρ is the fluid density. A similar relation holds that connects the mean velocity in the inner region, $U^{(i)}(x_{inl}, y) = \lambda^{(i)}_U\, U(x_{rec}, \lambda^{(i)}_U y)$, with a factor $\lambda^{(i)}_U$, also set equal to the ratio of friction velocities. In the outer region, an outer layer ratio $\lambda^{(o)}$ connects the variables between the planes in outer units, $y/\delta(x)$, i.e.

$$u'^{(o)}_i(x_{inl}, y, z, t) = \lambda^{(o)}_{u'}\, u'_i(x_{rec}, y\delta(x_{inl})/\delta(x_{rec}), z, t), \tag{2.4}$$

with possibly different ratios for different components ($\lambda^{(o)}_{u'}$, $\lambda^{(o)}_{v'}$ and $\lambda^{(o)}_{w'}$) and a similar expression for the mean velocity defect (Lund *et al.* 1998) that involves the ratio $\lambda^{(o)}_U$. The remaining challenge is to specify the values for the various λ factors.

For the inner region, the factor $\lambda^{(i)}_{u'} = (u_\tau)_{inl}/(u_\tau)_{rec}$ must be specified. While the stress (and thus $(u_\tau)_{rec}$) may be measured near the wall at the recycle station, the stress at

the inlet (and thus $(u_\tau)_{inl}$) is unknown. In Lund *et al.* (1998) this problem was solved by invoking an empirical law describing the evolution with downstream Reynolds number, i.e. taking the ratio of friction velocities to be equal to $(\theta_{rec}/\theta_{inl})^{1/2(n-1)}$, where n comes from the usual '$1/n$' power-law exponent of boundary layers and θ is the momentum thickness that is measured. A classic value of $n=5$ has often been used. However, since n is greatly impacted by pressure gradients and other effects such as possibly wall roughness and free-stream turbulence and also weakly by the Reynolds number, it is not justified to use $n=5$ in all cases. Therefore, this formulation for computing the friction velocity ratio is limited in principle to ZPG flows.

With the aim of avoiding having to specify such empirical parameters *a priori*, we recall the case of large-eddy simulation (LES). In LES, the dynamic approach by Germano *et al.* (1991) has provided a highly successful approach, by invoking a 'test filter' and interrogating simulated length scales of turbulence to determine unknown model parameters. In the present work, we propose a similar approach to obtain unknown model parameters for the inlet boundary condition. We begin by assuming a power-law variation of the friction velocity as $(u_\tau/U_\infty)\sim(Re_\delta)^\gamma$, where $Re_\delta=\delta U_\infty/\nu$, with ν the kinematic viscosity and δ denoting the boundary layer thickness, e.g. δ_{99} in which the velocity is 99 % of the free-stream velocity U_∞. By relating the friction velocity at the inlet station to that at the recycle station, we can write

$$\frac{(u_\tau/U_\infty)_{inl}}{(u_\tau/U_\infty)_{rec}}=\left(\frac{Re_{\delta\,inl}}{Re_{\delta\,rec}}\right)^\gamma, \tag{2.5}$$

where $(u_\tau)_{inl}$ and γ are unknowns. In order to find $(u_\tau)_{inl}$ from this expression, we must know γ. For ZPG boundary layers, the relationship between γ and the value n used in Lund *et al.* (1998) is $\gamma=1/[2(1-n)]=-1/8$ for $n=5$. The proposed methodology consists of determining the exponent γ dynamically. In analogy with the test-filter scale used in LES, we introduce a new plane, called the 'test plane', located between the inlet and recycle stations (figure 1), where the mean velocity gradient at the wall, and thus the friction velocity, can be measured. By applying the same expression to the test and recycle planes, the exponent γ may now be dynamically evaluated according to

$$\gamma=\frac{\ln[(u_\tau/U_\infty)_{test}/(u_\tau/U_\infty)_{rec}]}{\ln[Re_{\delta\,test}/Re_{\delta\,rec}]}. \tag{2.6}$$

One assumes that γ is constant along the computational domain, between the inlet and recycle planes. For cases in which the Reynolds number does not vary greatly, and the flow is in reasonable equilibrium during the downstream evolution, this assumption appears warranted. Once the exponent γ is obtained from (2.6), the value of $(u_\tau)_{inl}$ is calculated from (2.5). The free-stream velocities $(U_\infty)_{rec}$ and $(U_\infty)_{test}$ can be evaluated by averaging the mean streamwise velocity in the region above the boundary layer edge in the transverse direction. For ZPG flows, U_∞ is constant so that once γ is determined, in the special case of ZPG we obtain $\lambda_{u'}^{(i)}=(\delta_{inl}/\delta_{rec})^\gamma$. The parameter δ_{inl} is the prescribed inlet boundary layer thickness. Besides the free-stream velocity, δ_{inl} is the only parameter that needs to be prescribed at the inlet in this dynamic multi-scale approach.

For the scaling of the outer mean and fluctuating velocities, several options exist. The classic scaling uses the friction velocity, $\lambda_{u'}^{(o)}=(u_\tau)_{inl}/(u_\tau)_{rec}$. Conversely, other theories lead to other scales. For instance, the asymptotic invariance principle (George & Castillo 1997; Castillo & George 2001) leads to $\lambda_{u'}^{(o)}=\lambda_{w'}^{(o)}=(U_\infty)_{inl}/(U_\infty)_{rec}$ and $\lambda_{v'}^{(o)}=(U_\infty \mathrm{d}\delta/\mathrm{d}x)_{inl}/(U_\infty \mathrm{d}\delta/\mathrm{d}x)_{rec}$. Other scalings have been proposed, such

as the mixed scaling of DeGraaff & Eaton (2000) which would imply $\lambda_{u'}^{(o)} = (u_\tau U_\infty)_{inl}^{1/2}/(u_\tau U_\infty)_{rec}^{1/2}$. An interesting discussion about scaling laws in general pressure gradient flows can be found in Perry, Marusic & Jones (2002). The proposed dynamic approach may be applied to any of these formulations. For the outer region, here we explore applying it with the formulation of Castillo & George (2001). The specification of $\lambda_{v'}^{(o)}$ requires the rate of boundary layer growth $\mathrm{d}\delta/\mathrm{d}x$ at the inlet and its determination at the recycle plane. Measuring such derivatives from noisy data is challenging, and therefore we prefer to postulate power-law growth of $\delta(x)$ with respect to the x-coordinate Reynolds number ($Re_x = xU_\infty/\nu$), i.e. $(\delta/x) \sim (Re_x)^{\gamma_\delta}$. Again, by relating the inlet station to the recycle station, we can write

$$\frac{(\delta/x)_{inl}}{(\delta/x)_{rec}} = \left(\frac{Re_{x\,inl}}{Re_{x\,rec}}\right)^{\gamma_\delta}. \tag{2.7}$$

Then, the exponent γ_δ can be obtained dynamically by linking the corresponding quantities of the test and recycle planes as follows:

$$\gamma_\delta = \frac{\ln[(\delta/x)_{test}/(\delta/x)_{rec}]}{\ln[Re_{x\,test}/Re_{x\,rec}]}. \tag{2.8}$$

Finally, the boundary layer growth ratio is obtained as

$$\frac{(\mathrm{d}\delta/\mathrm{d}x)_{inl}}{(\mathrm{d}\delta/\mathrm{d}x)_{rec}} = \frac{\mathrm{d}\left(xRe_x^{\gamma_\delta}\right)_{inl}/\mathrm{d}x}{\mathrm{d}\left(xRe_x^{\gamma_\delta}\right)_{rec}/\mathrm{d}x}. \tag{2.9}$$

It is expected that the use of these scales can be applied to boundary layers with or without external pressure gradients.

At the test and recycle stations, one must obtain velocity gradients at the wall, as well as the boundary layer thickness from the mean velocity profiles. The assumed power-law behaviours for downstream evolution of friction velocity and boundary layer thickness refer to the properties of the mean velocity, not instantaneous realizations. Therefore, averaging procedures must be incorporated into the method. Since the flows considered in this paper have spanwise spatial homogeneity, spanwise averaging is performed. Still, time averaging is required to further reduce fluctuations. We use a linear relaxation process in which the time-filtered velocity $U(x, y, t_n)$, at time t_n corresponding to the time step n, is obtained according to

$$U(x, y, t_n) = (1 - \varepsilon)U(x, y, t_{n-1}) + \varepsilon\langle u(x, y, t_n)\rangle_z, \tag{2.10}$$

where $\langle u(x, y, t_n)\rangle_z$ is the velocity at the current time step, averaged in the z-direction, and ε is a small parameter, taken to be $\varepsilon = 1/N_{av}$. The selection of the number of averaging time steps, N_{av}, or averaging time, $N_{av}\Delta t$, is crucial and a compromise between a short transient and the desired level of noise in turbulent inflow information.

Additional smoothing is required when obtaining the boundary layer thickness. It has already been stated that δ_{inl} is the only parameter to be prescribed at the inlet on the basis of the desired inflow Reynolds number. However, δ at the test and recycle stations (needed in (2.6) and (2.8)) must be determined from the mean velocity profiles, where the velocity is 99 % of the free-stream value U_∞. To reduce oscillations on δ computations, the mean streamwise velocity profiles can be smoothed in the y-direction by using a spatial filter, in addition to the temporal filtering described above. This is similar to various averaging procedures that are often used in the Germano-identity-based dynamic subgrid model (Germano *et al.* 1991). Details of the implementation are described in the next section.

	ZPG		FPG	APG	
Parameter	Low Re_θ	High Re_θ	Moderate	Moderate	Strong
Re_θ	308–385	2667–3005	700	438–633	1029–1512
L_x/δ_{inl}	10.7	10	15	15	12
L_y/δ_{inl}	3	3	3	3.8	3
L_z/δ_{inl}	1.7	1.6	3	1.6	3.2
$N_x N_y N_z$	$90 \times 50 \times 40$	$400 \times 150 \times 125$	$200 \times 120 \times 120$	$120 \times 65 \times 50$	$150 \times 90 \times 100$
Δx^+	18.9	20	20	20	21
$\Delta y^+_{min}/\Delta y^+_{max}$	0.5/13	0.5/20	0.2/15	0.2/6.8	0.2/17
Δz^+	6.77	10	8	5	8
Δt^+	0.63	0.44	0.36	0.59	0.22
$T_{sample}\frac{u_\tau^2}{\nu}$	1890	2200	1080	1770	1540
δ^+_{inl}	152	980	446	161	271

TABLE 1. Proposed DNS cases and domain parameters for various pressure gradients.

3. Applications

Direct numerical simulations of the Navier–Stokes equations for incompressible flow are performed using the Parallel Hierarchic Adaptive Stabilized Transient Analysis code. It is based on the finite-element method with a streamline upwind Petrov–Galerkin stabilization. A weak formulation of the problem results in a system of nonlinear ordinary differential equations, which are discretized in time via a generalized-α time integrator producing a nonlinear system of algebraic equations. This system is, in turn, linearized with Newton's method which yields a linear algebraic system of equations. Additionally, the fully coupled momentum and continuity equations are solved with multiple nonlinear iterations and an additional discrete pressure Poisson equation between each iteration, to maintain a tight tolerance on continuity. Two nonlinear iterations are performed on each step. More details about the code can be found in Jansen (1999) and Whiting & Jansen (2001), as well as some applications in Trofima *et al.* (2009) and Tejada-Martinez & Jansen (2005, 2006).

Regarding the inlet boundary condition, and as in Lund *et al.* (1998) and every other application of a recycling boundary condition, the velocity profiles from the recycle plane are deformed in the wall-normal direction but not in the other directions. As a consequence, the reinjected velocity field is not exactly divergence-free at the inlet plane. However, deviations from zero divergence are small because of the slow variations in time of the convective velocity, the relatively small fractional vertical rescaling and the use of a fully implicit method with multiple nonlinear iterations and tight tolerance on continuity. Therefore, at the first plane after the inlet, the divergence-free condition has already been fully restored up to the imposed tolerance. We have experimented with higher numbers of nonlinear iterations and tighter solver tolerances and shown that these do not affect the results shown. Periodic boundary conditions are prescribed in the spanwise direction.

Table 1 summarizes the different simulation cases, covering various levels of pressure gradients (ZPG, FPG and APG) and Reynolds numbers (i.e. $308 \leqslant Re_\theta \leqslant 3005$). The corresponding domain dimensions and mesh resolutions are also shown. A grid independence test as well as a sensitivity analysis of domain dimensions have already been performed in Araya *et al.* (2009). In the wall-normal direction, non-uniform mesh sizes are used with the minimum near-wall and maximum outer vertical resolutions indicated in table 1.

The recycle plane is located far downstream from the inlet, at approximately 80 % of the streamwise domain length in all cases. This ensures an almost zero value for the two-point correlation (see the analysis in the Appendix) of fluctuating velocities between these two planes, and it allows the turbulent structures to evolve relatively independent of the recycle plane conditions. The test plane is situated halfway between the inlet and recycle planes, and its only function is the determination of the corresponding powers from (2.6) and (2.8) by relating the flow solutions at the test and recycle stations. In this way, the friction velocity at the inlet is determined independent of *ad hoc* parameters from theory or empirical scaling laws.

Recent studies carried out by several groups including Balakumar & Adrian (2007), Guala, Hommema & Adrian (2006), Mathis, Hutchins & Marusic (2009) and Hutchins & Marusic (2007*a*,*b*) have shown the importance of large-scale structures that extend significantly in the streamwise direction of wall-bounded turbulent flows. These include scales identified through spectral analysis that are of length $O(6\delta)$ and observations in physical space of even longer structures ('super-structures') of length $O(10\text{–}20\delta)$. An implication from these studies is that the computational domain must be long enough in the streamwise direction to capture the spectral scales, as discussed in the study of Hutchins & Marusic (2007*b*), and ideally the super-structures as well. As shown in the second row of table 1, the ratio L_x/δ_{inl} falls in a range of 10–15, providing clear evidence that spectral scales ($O(6\delta)$) are well resolved and that some of the super-structures (of length $\sim 10\delta_{inl}$) are properly captured in the simulations as well. In addition, a two-point correlation analysis can be used to quantify the couplings among the inlet and outlet regions in the computational domain. These considerations are presented in detail in the Appendix for the ZPG, FPG and APG flow simulations. The analysis shows that the autocorrelations decay in the streamwise direction sufficiently quickly to support the adequacy of the domain lengths used in this study. For instance, in the present two-point correlations, we observe that streamwise fluctuation correlations R_{uu} are approximately uncorrelated by $x^+ \approx 500$ in most cases considered (and $x^+ \approx 1000$ for the high-Reynolds-number ZPG case). These decorrelation scales correspond to about 15–25 % of the length of the computational domain. We caution that if DNS is carried out with the specific purpose of studying the detailed dynamics of very long streamwise super-structures, longer domains should be used (i.e. of the order of $20\text{–}30\delta_{inl}$) to make sure that the longest structures are resolved without any possibilities of inflow–outflow coupling. For such applications, the dynamic inflow boundary condition approach proposed in this work can be applied with the required longer domains as well, still providing significant savings compared with having to simulate the full laminar–transition regimes.

In order to accelerate convergence, reduce initial transients and help maintain simulation stability, it has been found convenient to fix the mean part of the inlet streamwise velocity profile for some initial time before allowing it to adjust dynamically. The prescribed fixed mean profile is obtained from the theory of George & Castillo (1997) for ZPG flows. During the initialization stage, the wall-normal and spanwise components of the mean velocity and all the fluctuations are rescaled from the recycle plane according to the proposed dynamic method. After the transients have died down, the mean streamwise velocity from the recycle plane is also rescaled and prescribed at the inflow. The reader is referred to page 8 of Araya *et al.* (2009) for further details about the initial conditions and start-up stage. During the start-up process it has been found convenient to clip the λ values between reasonable top and bottom limits (we use $0.5 < \lambda < 1.5$). The start-up stage in present simulations is chosen to last about 6000–7000 viscous time scales.

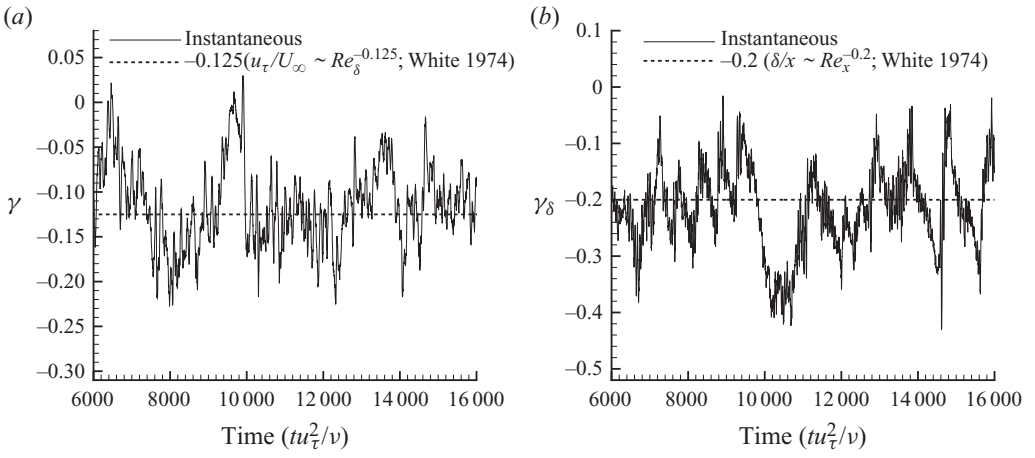

FIGURE 2. Time series of the dynamically computed power-law exponents for a low-Reynolds-number ZPG boundary layer: (*a*) the friction velocities and (*b*) the boundary layer thickness.

For the time smoothing via time averaging, a value of N_{av} must be prescribed. It was found that a value of $N_{av} = 10^3$ was appropriate for the low- to moderate-Reynolds-number cases. In physical units, this corresponds to about 220–600 viscous time scales, depending on the flow cases considered. In outer units, it corresponds to about $78(\delta/U_\infty)_{inl}$. In the ZPG case at higher Reynolds numbers, a value of 7×10^3 for N_{av} was prescribed, which matches the averaging time of the ZPG case at lower Reynolds numbers in outer units, i.e. also $78(\delta/U_\infty)_{inl}$. To determine δ from the mean velocity profile in the outer part, spatial filtering of the mean streamwise velocity profiles in the y-direction is done using a five-point averaging window, i.e. two points above and two below any given height. This smoothing procedure was applied only at the boundary layer edge to compute the boundary layer thickness at the test and recycle planes but was not performed either on the composite inlet velocity profile (2.1) or in the final statistics calculation.

3.1. *ZPG boundary layer*

Figure 2(*a*) shows a representative time series of the dynamically computed power-law exponent γ obtained as in (2.6) for the case of a ZPG boundary layer at a low Reynolds number. It is observed that γ fluctuates significantly, around the classical empirical value of -0.125 (see e.g. White 1974) shown as the dashed line. Figure 2(*b*) shows the time series of γ_δ for the boundary layer thickness from which the growth rate is computed. Similarly, γ_δ fluctuates around the classical empirical value of -0.2 (White 1974). It is encouraging that for the case of ZPG, the dynamic approach yields values that agree with the expected well-known empirical values. Figure 3(*a*) depicts the time variation of γ based on (2.6) for the ZPG case at high Reynolds numbers up to $Re_\theta \sim 3000$. It is observed that the instantaneous value of γ fluctuates more strongly than in the smaller-Reynolds-number case. Such fluctuations can be large because the exponents γ are ratios of averages and thus are susceptible to fluctuations of both the numerator and the denominator. There is some periodicity in the exponent fluctuations for the case of γ_δ in the high-Reynolds-number case, which seems to occur at a time scale of the order of the averaging time scale. But these oscillations do not translate into oscillations of the λ factors (see below). It is worth recalling that in the implementation the only temporarily filtered and spanwise-averaged variable is the streamwise velocity by means of (2.10). The computed γ values from (2.6) and

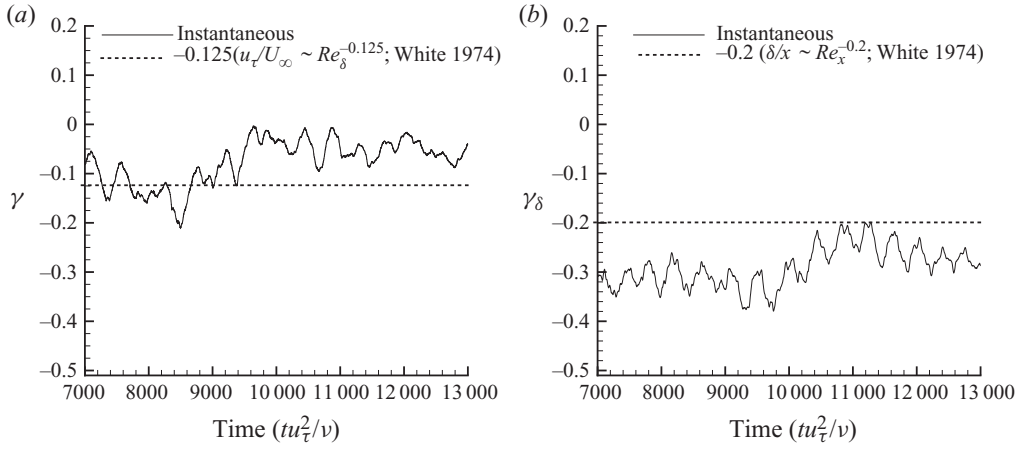

FIGURE 3. Time series of the dynamically computed power-law exponents for a high-Reynolds-number ZPG boundary layer: (*a*) the friction velocities and (*b*) the boundary layer thickness.

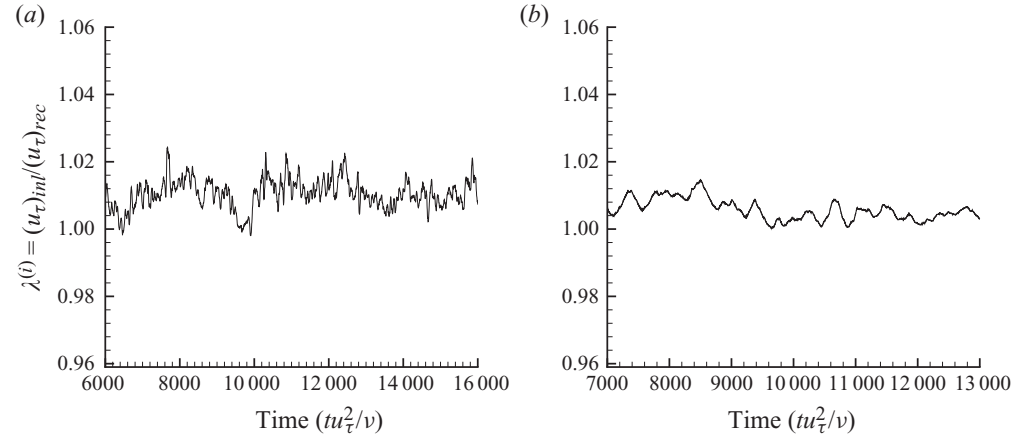

FIGURE 4. Time variation of the friction velocity ratio at the inlet plane to the recycle station for (*a*) low and (*b*) high Reynolds numbers.

(2.8) are not filtered *a posteriori*. The level of fluctuations could be reduced in future applications by increasing N_{av} (decreasing ε) in the time-averaging process of the velocity.

The λ factors, which directly enter in the rescaling process, do not fluctuate as much as the values of γ do because of cancellations that occur through variations of other parameters such as the boundary layer thickness and free-stream velocity. The time series of $\lambda^{(i)} = (u_\tau)_{inl}/(u_\tau)_{rec}$ are shown in figure 4. As can be seen, typical values obtained are between 1 % and 4.5 % change with respect to $\lambda = 1$. In terms of stresses, these represent downstream changes between 2 % and 10 %. We also observe that the value of γ_δ at high Reynolds numbers is lower than the expected −0.2 based on White (1974). Still, as will be seen below, the resulting flow statistics are quite realistic. Figure 5(*a*) presents the streamwise development of the boundary layer thickness δ and the shape factor $H = \delta^*/\theta$ as a function of the momentum thickness Reynolds number Re_θ for the low-Reynolds-number ZPG simulations.

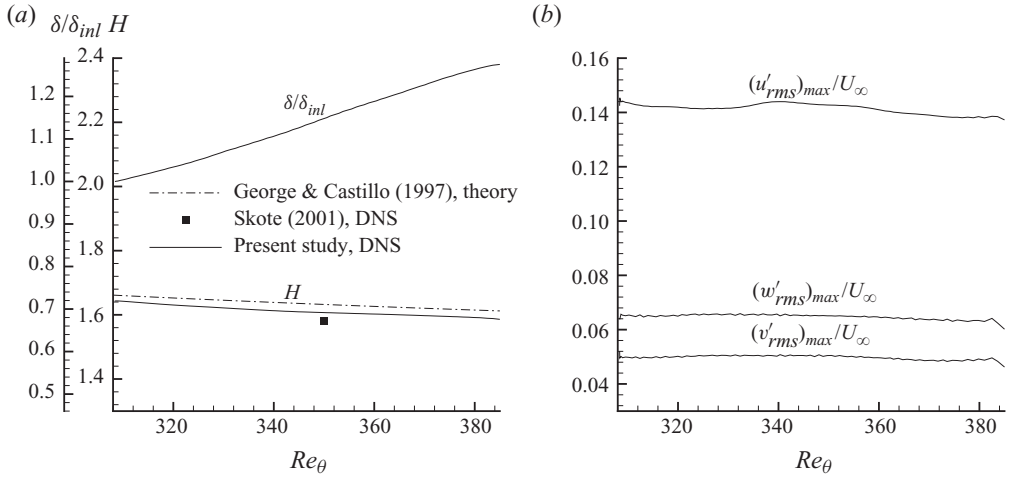

FIGURE 5. Streamwise development of some boundary layer parameters in ZPG flows for low Reynolds numbers: (*a*) δ/δ_{inl} and H; (*b*) local maxima of velocity fluctuations.

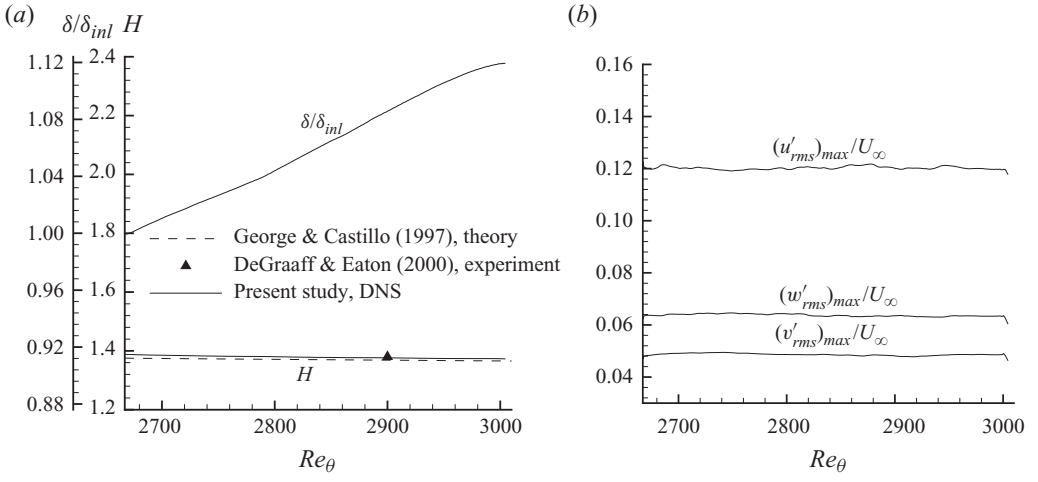

FIGURE 6. Streamwise development of some boundary layer parameters in ZPG flows for high Reynolds numbers: (*a*) δ/δ_{inl} and H; (*b*) local maxima of velocity fluctuations.

There is a good agreement of the present values of H with the theory of George & Castillo (1997) and the DNS data from Skote (2001). The local maxima of velocity fluctuations normalized by the free-stream velocity (i.e. $(u'_{rms})_{max}/U_\infty$, $(v'_{rms})_{max}/U_\infty$ and $(w'_{rms})_{max}/U_\infty$) are shown in figure 5(*b*). As can be seen, $(u'_{rms})_{max}/U_\infty$ shows a small bump near $Re_\theta \approx 340$ (streamwise length of approximately $4.7\delta_{inl}$), which suggests that the fluctuations are still recovering from the inlet condition even when mean boundary layer parameters, such as δ and H, are fully equilibrated in this region. Figure 6(*a*) shows the streamwise growth of the boundary layer thickness for the high-Reynolds-number case. The computed shape factor H, also shown in figure 6(*a*), agrees very well with the experiments of DeGraaff & Eaton (2000) and the theory of George & Castillo (1997). The ratios of velocity fluctuation maxima to free-stream velocities are approximately constant along the entire domain (figure 6*b*) without an

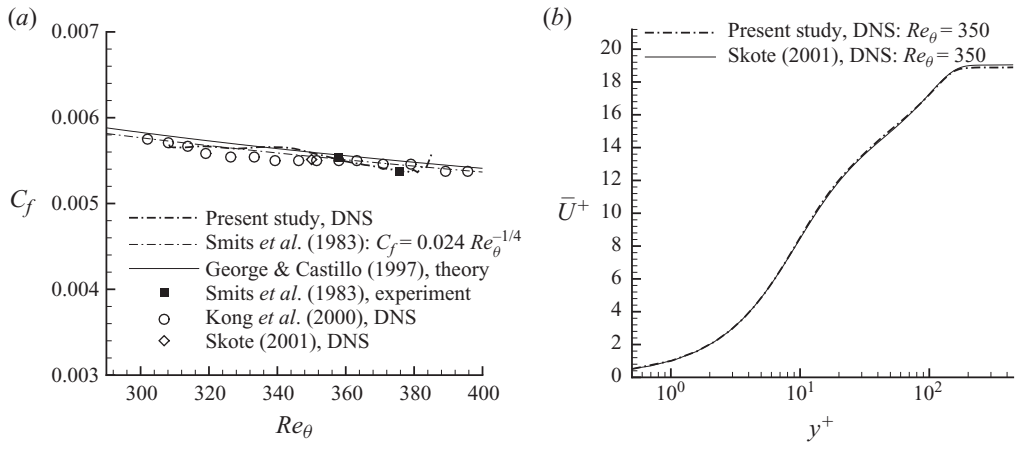

FIGURE 7. (*a*) Streamwise variation of the skin-friction coefficient in a low-Reynolds-number ZPG boundary layer and comparison with the existing data and $-1/4$ scaling law and (*b*) mean streamwise velocity in wall units and comparison with the results of Skote (2001).

obvious developing section. The ratio $(u'_{rms})_{max}/U_\infty$ is found to be near 12 %, whereas the same ratio was found to be near 14 % in the low-Reynolds-number simulations.

Next, the downstream evolution of mean velocity near the wall is documented by computing the wall stress from $\partial U/\partial y$ at the wall, obtaining the friction velocity, measuring the momentum thickness and plotting $C_f = 2(u_\tau/U_\infty)^2$ as function of Re_θ in figure 7(*a*). It is observed that no transient or adjustment region is visible near the inlet in the C_f plot. Furthermore, the computed skin-friction coefficient in figure 7(*a*) is in good agreement with the DNS data from Skote (2001) (at $Re_\theta = 350$) and Kong, Choi & Lee (2000), the experiments from Smits, Matheson & Jourbert (1983), the empirical correlation from Smits *et al.* (1983) for low Reynolds numbers and the power law theory of George & Castillo (1997). Maximum errors were found to be within 3 %. There is a small 'uptick' at the end of the domain, caused by the prescribed pressure outflow boundary condition. However, the recycle plane is selected sufficiently far away from the outflow that the flow solution is not affected at this recycling station.

Turning to vertical profiles, in figure 7(*b*) the mean streamwise velocity profile for the $Re_\theta = 350$ case is shown. It overlaps the velocity profile computed by Skote (2001) very well. The corresponding root mean square (r.m.s.) values of velocity fluctuations are shown in figure 8(*a*) in inner variables. In general, the comparison with the data of Skote (2001) is quite good, only that the presently computed peak values of u'^+_{rms} are approximately 4 % larger. The Reynolds shear stresses are plotted in figure 8(*b*). The agreement with the results of Skote (2001) at the same Reynolds number is excellent over the entire boundary layer. These results provide evidence that the prescribed inlet velocity profile obtained from the dynamic rescaling–recycling method is realistic. Notice that Skote (2001) started the simulations from a laminar profile and triggered the flow to become turbulent. Hence, a much longer computational domain size was needed. The streamwise domain size used in this work is about 5 times shorter. A successful grid-independence test of a similar simulation case (ZPG at low Reynolds numbers, but using a non-dynamic recycling approach) was performed in Araya *et al.* (2009). They also presented comparison with a much longer domain.

For the high-Reynolds-number ZPG simulations, figure 9(*a*) shows the skin-friction coefficient as a function of Re_θ. The results are generally in good agreement with the theoretical profile of George & Castillo (1997), the empirical correlation of

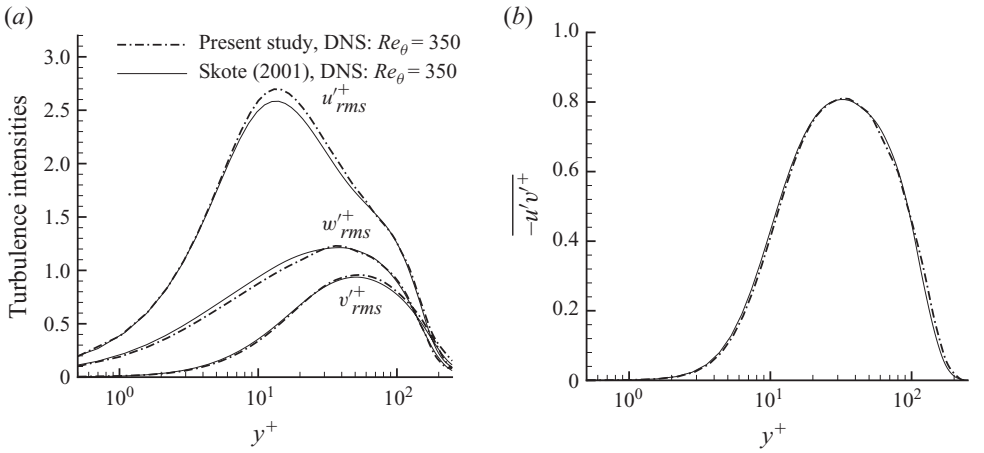

FIGURE 8. Profiles of (*a*) turbulence intensities and (*b*) Reynolds shear stresses in wall units for DNS of a low-Reynolds-number ZPG boundary layer.

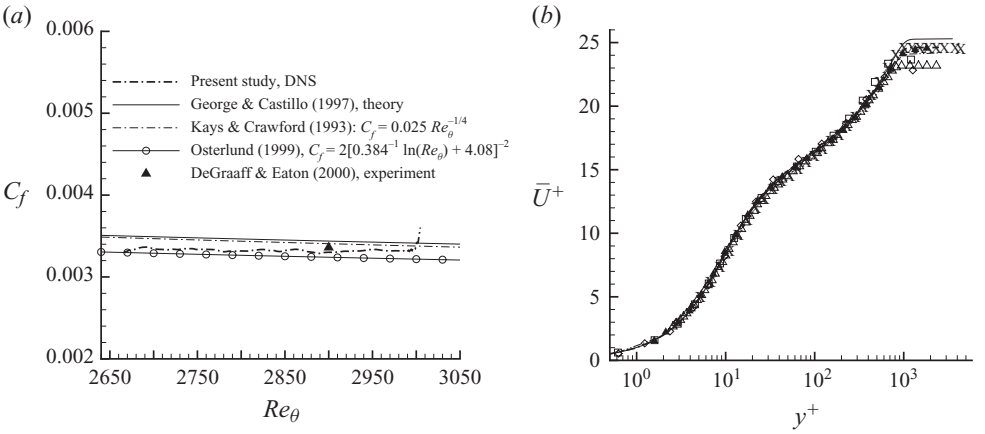

FIGURE 9. (*a*) Streamwise variation of the skin-friction coefficient in a high-Reynolds-number ZPG boundary layer and (*b*) the mean streamwise velocity in wall units. (*b*) Lines and symbols: (–·–·–), Present study, DNS: $Re_\theta = 2900$; (◇), Lund *et al.* (1998), *LES*: $Re_\theta = 1850$; (□), Simens *et al.* (2009), DNS: $Re_\theta = 1968$; (△), Khujadze & Oberlack (2004), DNS: $Re_\theta = 2240$; (X), Österlund (1999), experiment: $Re_\theta = 2533$; (▲), DeGraaff & Eaton (2000), experiment: $Re_\theta = 2900$; (–··–··–), Ferrante & Elghobashi (2005), DNS: $Re_\theta = 2900$; (————), Schlatter *et al.* (2009), DNS: $Re_\theta = 3274$.

Kays & Crawford (1993) for high Reynolds numbers, the experimental results of DeGraaff & Eaton (2000) and the proposed empirical function of Osterlund (1999). Figure 9(*b*) shows the results for the mean streamwise velocity in wall units at $Re_\theta = 2900$. The agreement with the experimental results of DeGraaff & Eaton (2000) and the DNS of Ferrante & Elghobashi (2005) at similar Re_θ is excellent. Similarly, a good collapse with the LES results of Lund *et al.* (1998), the DNS of Simens *et al.* (2009), Khujadze & Oberlack (2004) and Schlatter *et al.* (2009) and the experiments from Osterlund (1999) can be appreciated, except in the wake region because of the different Reynolds numbers involved. The turbulence intensities (i.e. u'^+_{rms}, v'^+_{rms} and w'^+_{rms}) are shown in figure 10(*a*) in inner–outer variables at $Re_\theta = 2900$. The agreement with the experiments of DeGraaff & Eaton (2000) and the DNSs of Ferrante & Elghobashi (2005), Simens *et al.* (2009) and Schlatter *et al.* (2009) is quite

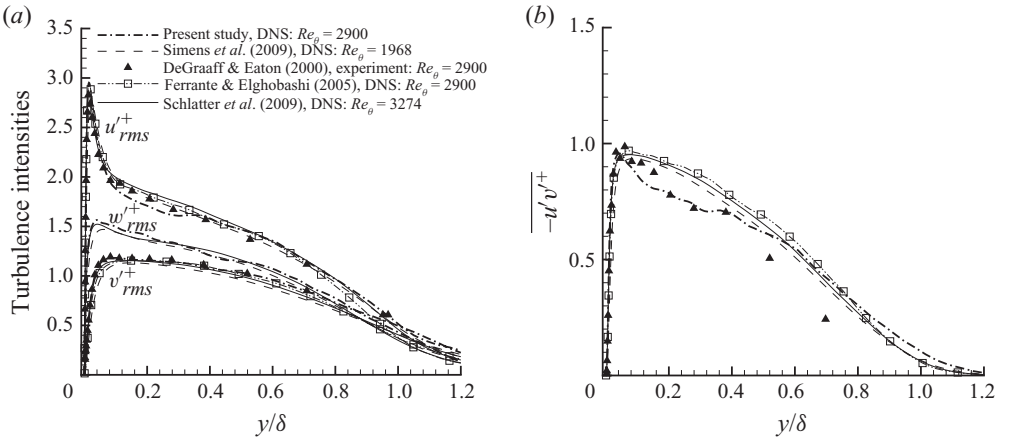

FIGURE 10. Profiles of (*a*) turbulence intensities and (*b*) Reynolds shear stresses in wall units for DNS of a high-Reynolds-number ZPG boundary layer.

good, particularly with the results of the experiments that were performed at the same Re_θ. The most significant discrepancies can be observed in the peak of u'^+_{rms} ($\sim$3.5 %). The Reynolds shear stresses $-\overline{u'v'}^+$ are plotted in figure 10(*b*) together with the experiments of DeGraaff & Eaton (2000) and the DNS of Ferrante & Elghobashi (2005), Simens *et al.* (2009) and Schlatter *et al.* (2009). Our data show a better agreement with DeGraaff & Eaton (2000) in the inner region (up to $y/\delta \sim 0.4$). However, the present values of the Reynolds shear stresses are significantly higher than those of DeGraaff & Eaton (2000) in the outer layer (i.e. $y/\delta > 0.4$), and a better match with the predictions of Ferrante & Elghobashi (2005), Simens *et al.* (2009) and Schlatter *et al.* (2009) is appreciated in this region. It should be pointed out that the present shear-stress profile displays some remaining fluctuations due to lack of full statistical convergence. The prior results by Simens *et al.* (2009) and Schlatter *et al.* (2009) display less fluctuations because of larger averaging samples in the case of Schlatter *et al.* (2009) and additional streamwise averaging (between $Re_\theta = 1938$ and $Re_\theta = 1996$) in the case of Simens *et al.* (2009).

In comparing the computational cost associated with the domain length, we point out that the simulations of Schlatter *et al.* (2009) used a laminar inlet profile that was triggered to transition to turbulent conditions, as in Skote (2001), requiring a computational domain roughly 9 times larger than ours. The domain employed by Simens *et al.* (2009) was roughly 4.7 times longer than that used in present simulations.

3.2. *FPG boundary layer*

The dynamic rescaling–recycling method is also tested in a moderate-FPG flow, generated by a boundary layer under a top convergent straight wall (sink flow). The dimensionless pressure gradient parameter $K = \nu/U_\infty^2\, \mathrm{d}U_\infty/\mathrm{d}x$ remains approximately constant and equals 1.5×10^{-6}. To simplify the implementation for the pressure gradient simulations, the wall-normal components of the velocity have been scaled only by U_∞ in the outer layer. Hence, we do not need to determine dynamically the exponent γ_δ. The assessment of using the scale $U_\infty \mathrm{d}\delta/\mathrm{d}x$ and determining γ_δ dynamically also in pressure gradient flows is left as a task for future studies.

Figure 11 shows the time variation of the dynamically computed γ (2.6). It is observed that γ oscillates around zero; consequently, the ratio u_τ/U_∞ is nearly

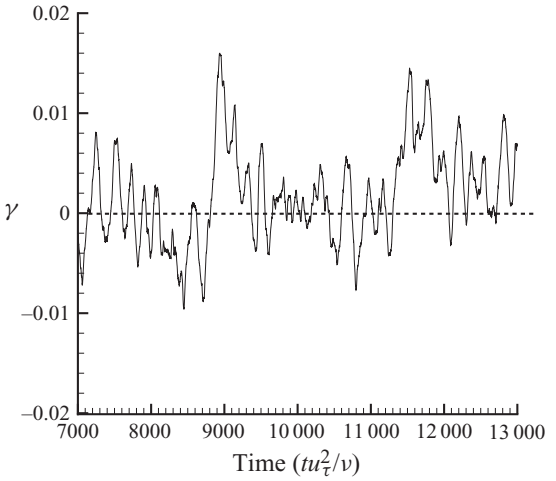

FIGURE 11. Time series of the dynamic exponent γ for an FPG boundary layer.

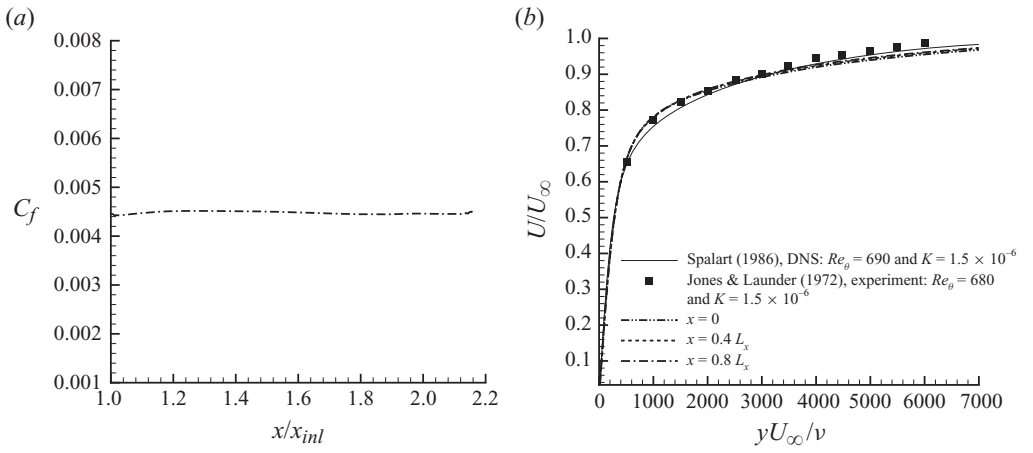

FIGURE 12. (*a*) Downstream evolution of the skin friction. (*b*) Mean velocity profiles at three downstream stations and comparison with earlier data.

constant along the streamwise direction. This is consistent with the expected constant value for the skin-friction coefficient C_f, as shown in figure 12(*a*). Similarly, the momentum thickness Reynolds number Re_θ exhibits a constant value of approximately 700 after a short initial transient (not shown). In figure 13(*a*), the boundary layer thickness δ exhibits a nearly linear decreasing behaviour typical in sink flows. And the shape factor H is almost constant and equal to 1.4 in the entire computational domain. The local streamwise and spanwise velocity fluctuations display some entrance effects over roughly 18 % of the domain, or $3\delta_{inl}$, as observed in figure 13(*b*). The local maxima of wall-normal velocity fluctuations show less entrance effects.

The mean streamwise velocity profiles shown in figure 12(*b*) are normalized by the local free-stream velocity U_∞ and plotted at three different x streamwise locations: 0, $0.4L_x$ and $0.8L_x$, i.e. the inlet, test and recycle planes, respectively. The collapse of profiles is excellent, even for the inlet velocity profile. Furthermore, a comparison

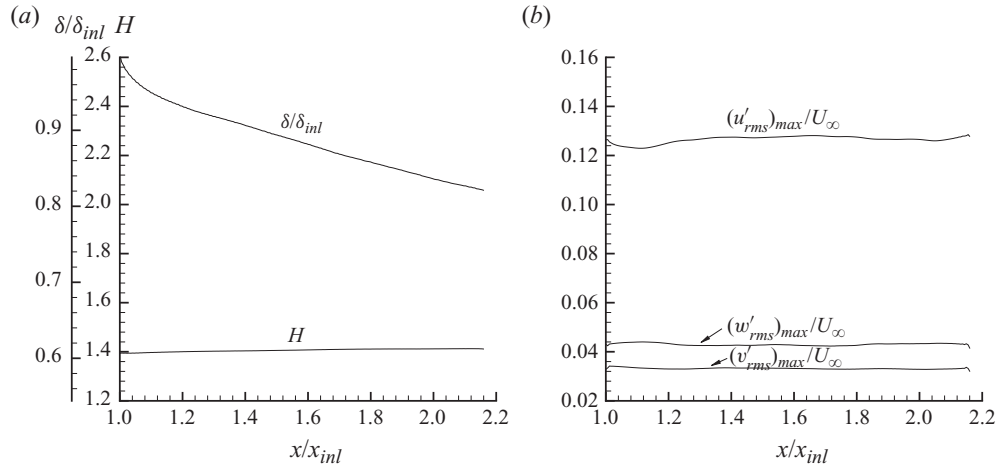

FIGURE 13. Streamwise development of some boundary layer parameters in FPG flows: (*a*) δ/δ_{inl} and H; (*b*) local maxima of velocity fluctuations.

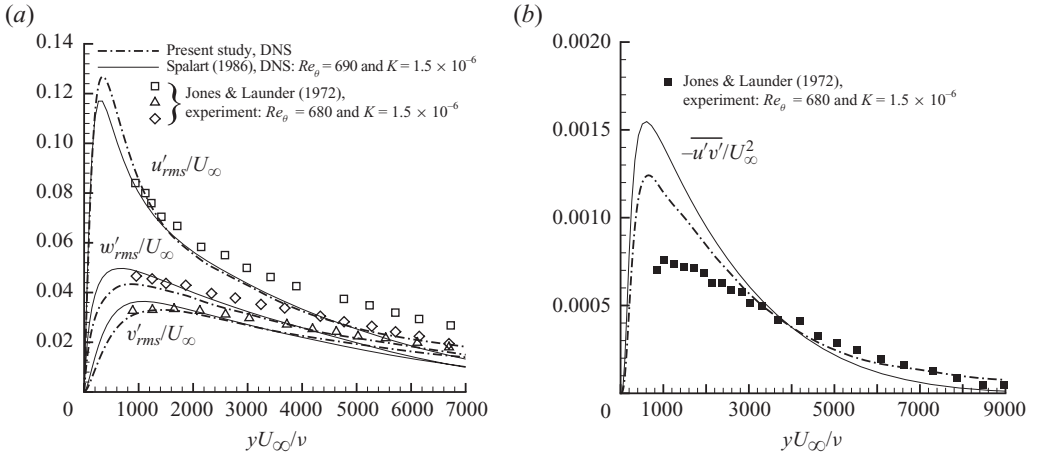

FIGURE 14. (*a*) Turbulence intensities and (*b*) Reynolds shear stresses in outer units for DNS of an FPG boundary layer, using the dynamic multi-scale rescaling–recycling method.

is performed with the DNS data from Spalart (1986) and the experimental results by Jones & Launder (1972) in sink flows for similar Re_θ and K values. Maximum discrepancies with the data are less than 3 %. Turbulence intensities are depicted at $x = 0.8L_x$ in figure 14(*a*) and are also normalized by the local U_∞. Generally speaking, our results exhibit good agreement with prior data, and slightly better agreement is seen with the results of Spalart (1986). Furthermore, the maxima of v'^{+}_{rms} and w'^{+}_{rms} in the present DNS are very close to the ones obtained by Jones & Launder (1972), but their data do not reach the peak of u'^{+}_{rms}. The Reynolds shear stresses $\overline{u'v'}/U_\infty^2$ are plotted in figure 14(*b*) together with the DNS from Spalart (1986) and the experiments from Jones & Launder (1972). Our results produce peak values in between both existing data sets. Specific causes for the differences will require further, more detailed exploration. In the outer region, present simulation results for $-\overline{u'v'}/U_\infty^2$ agree better with the experiments of Jones & Launder (1972).

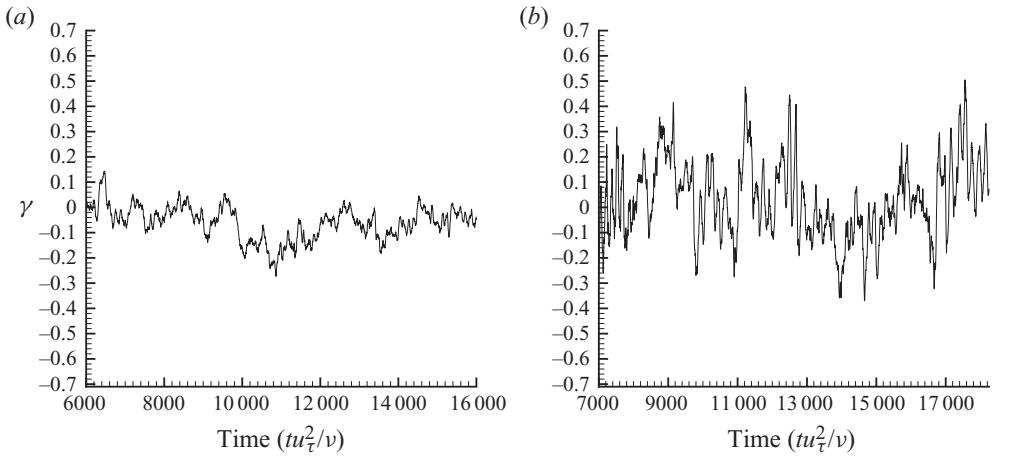

FIGURE 15. Time series of the dynamically computed power-law exponents for the friction velocities in APG flows: (*a*) moderate and (*b*) strong.

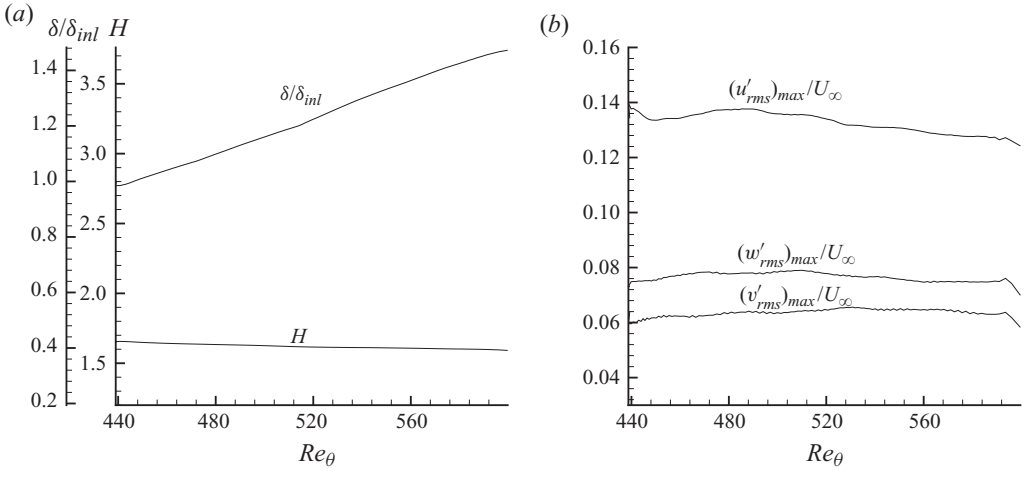

FIGURE 16. Streamwise development of some boundary layer parameters in moderate-APG flows: (*a*) δ/δ_{inl} and H; (*b*) local maxima of velocity fluctuations.

3.3. *APG boundary layers*

For simulations of moderate and strong APGs, the curvature at the upper surface of the computational box is prescribed in such a way as to obtain a power-law variation of the free-stream velocity, i.e. $U_\infty \sim (x - x_o)^m$ with $m = -0.17$ and -0.22, respectively.

Figure 15 show the representative time series of the dynamically computed power-law exponent γ for the friction velocities in the moderate- and strong-APG cases. As can be seen, the fluctuations of γ for the strong case are significantly higher than those for the moderate case. This is consistent with the overall larger level of variability in the strong-APG flow and the higher Reynolds number. In addition, the streamwise development of some boundary layer parameters (δ and H) are depicted in figures 16(*a*) and 17(*a*). The boundary layer thickness δ exhibits an almost-linear increasing trend, as is expected in these types of APG flows where the free-stream velocity follows a power law. A non-negligible developing section with a length of

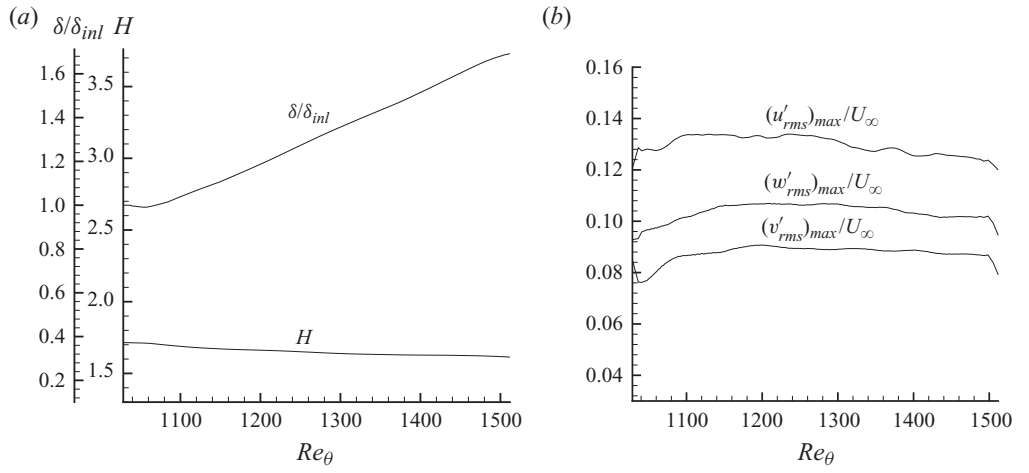

FIGURE 17. Streamwise development of some boundary layer parameters in strong-APG flows: (*a*) δ/δ_{inl} and H; (*b*) local maxima of velocity fluctuations.

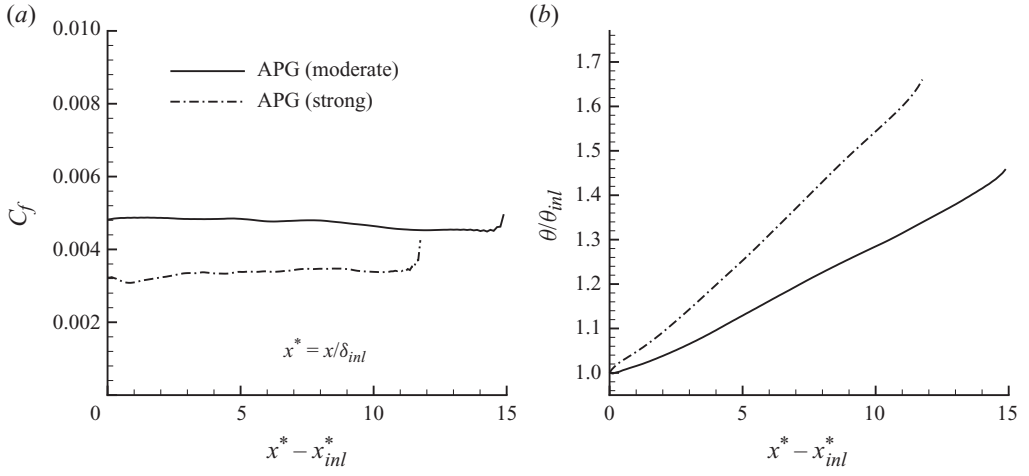

FIGURE 18. Downstream evolution of (*a*) C_f and (*b*) θ/θ_{inl} for both moderate and strong APGs.

approximately $1\delta_{inl}$ is observed for the strong-APG case. The shape factor H varies between 1.71 and 1.62 for the range of Re_θ (∼438–633) considered in the moderate-APG case with $m = -0.17$. It is encouraging to see close agreement with Skote (2001), who obtained a value of $H \sim 1.625$ at $Re_\theta \approx 685$ in a similar APG flow ($m = -0.15$).

The local maxima of velocity fluctuations scaled by the local free-stream velocity (i.e. $(u'_{rms})_{max}/U_\infty$, $(v'_{rms})_{max}/U_\infty$ and $(w'_{rms})_{max}/U_\infty$) are shown in figures 16(*b*) and 17(*b*) for the moderate- and strong-APG cases, respectively. An initial adjustment section is also observed with lengths of approximately $4\delta_{inl}$ in both APG cases. Furthermore, downstream of the adjustment section, a decreasing behaviour of $(u'_{rms})_{max}/U_\infty$ can be observed, as expected in a decelerating boundary layer.

The skin-friction coefficient evolutions, plotted in figure 18(*a*), depict an initial adjustment region, which is slightly longer for the strong APG. Downstream, the C_f profiles decrease very slowly, particularly for the strong-APG flow. Note that the

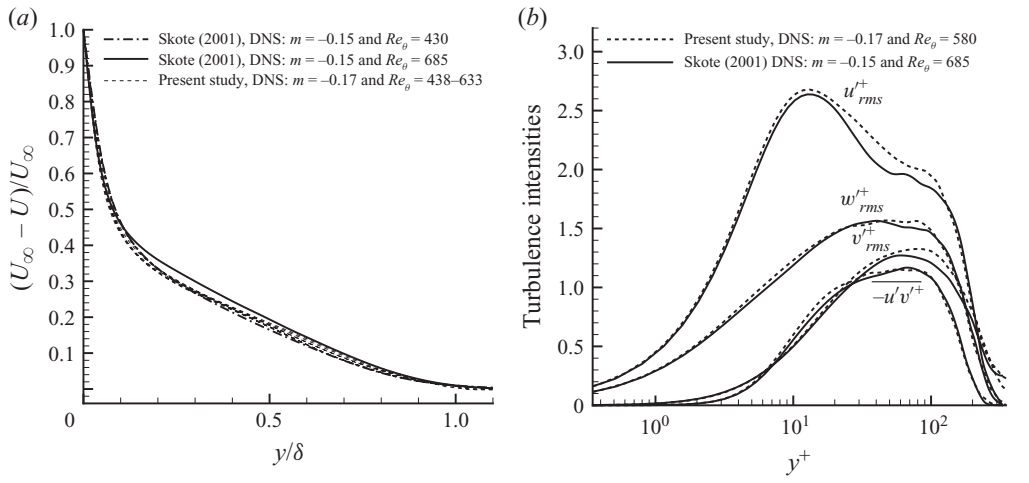

FIGURE 19. (*a*) Mean streamwise defect velocity and (*b*) turbulence intensities and Reynolds shear stresses in inner units from DNS of a moderate-APG flow.

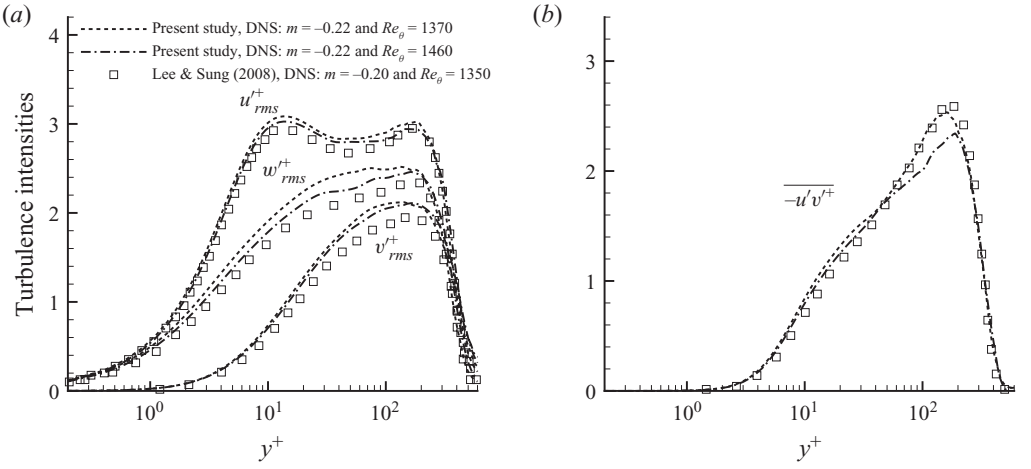

FIGURE 20. (*a*) Turbulence intensities and (*b*) Reynolds shear stresses for simulations of strong APG.

upticks at the end of the domain are more evident here than for the ZPG case. The momentum thickness θ plotted in figure 18(*b*) exhibits an almost-linear trend in both cases. We recall that a linear growth is one of the main expected characteristics of equilibrium APG boundary layers.

In figure 19(*a*), the mean streamwise defect velocity profiles are shown in outer units for moderate APG, normalized by the local free-stream velocity, at several downstream positions. A good collapse of all profiles is observed. Furthermore, good agreement can be observed with the data from Skote (2001) that was at a lower Re_θ but for the same value of $m = -0.15$. The turbulence intensities (u'^+_{rms}, v'^+_{rms} and w'^+_{rms}) and Reynolds shear stresses ($-\overline{u'v'}^+$) are shown in figure 19(*b*) at $Re_\theta = 580$. The pressure gradient effects are mostly manifested in the region around $y^+ \approx 100$, as peaks or 'shoulders' in the profiles. This behaviour is even more evident in streamwise velocity fluctuations u'^+_{rms}. As the APG becomes stronger, in figure 20(*a*) the outer

peak in u'^{+}_{rms} at $y^{+} \approx 200$ is almost as high as the inner peak in u'^{+}_{rms} at $y^{+} \approx 10$. Notice that the maxima of the Reynolds shear stresses ($-\overline{u'v'}^{+}$), shown in figures 19(b) and 20(b), move away from the wall as the APG strength increases. It is also observed that, as expected, the stress profile has a slope given by the pressure gradient, which becomes very steep for the strong-APG case. Moreover, comparing the present velocity fluctuations with the simulations by Skote (2001) and Lee & Sung (2008) at similar Reynolds numbers (Re_θ) and APG strength (m), we see that the agreement is quite good, particularly for the $Re_\theta = 1370$ case which matches the Reynolds number of Lee & Sung (2008). The good agreement is particularly encouraging considering that the streamwise domain lengths of these prior studies by Skote (2001) and Lee & Sung (2008) were 4 and 14 times larger, respectively, than those of the presently reported simulations using the dynamic rescaling–recycling method.

4. Conclusions

A generalized rescaling–recycling method has been proposed and tested. The method enables the use of different velocity scaling parameters in different regions of boundary layers, and unknown scaling exponents have been dynamically determined using information from the downstream evolution in the simulation. The proposed approach opens up the possibility to simulate spatially evolving boundary layers under more general pressure gradient situations, because empirical correlations are not needed to be known *a priori*. The approach has been shown to yield reasonable exponents for cases in which they are already known empirically (such as ZPG). Applications to FPG and APG flows have yielded realistic results with relatively short adjustment regions near the inlet of the computational domains. The adjustment region was found to be quite short for the mean velocity profile characteristics such as boundary layer thicknesses and shape factors, but longer for parameters associated with turbulent fluctuations, such as peak r.m.s. values.

The proposed method has several limitations that are important to appreciate. One is the assumption that the scaling exponents that are relevant between the inlet and recycle planes are the same as between the test and recycle planes. Therefore, the method is not expected to be applicable to flows with strong non-equilibrium transitions between the planes used in the dynamic approach. For instance, if the flow separates or relaminarizes somewhere between the inlet and recycle planes naturally, the method cannot be applied. For such cases, the method could be used to generate inflow in a separate simulation with near-equilibrium conditions, which could then be employed to feed data into a main simulation domain under more general conditions. The strength of the method lies in the fact that it becomes possible to simulate high-Reynolds-number boundary layers (results at $Re_\theta = 2900$ have been shown for ZPG flows) at a significantly lower cost, without having to simulate the entire laminar–transition–turbulent region. As in the method of Lund *et al.* (1998), another limitation is that rescaling is done only in the vertical direction. This is appropriate for the mean velocity field. The fluctuations, however, include structures whose characteristic spanwise length scales also develop downstream. The same is true for the characteristic time scales. However, reinjecting fields that have been rescaled in the z-direction would appear to be challenging, especially using periodic boundary conditions, and temporal rescaling appears even more difficult without the storing and processing fields at different times. Such further generalizations could be considered in future improvements of the recycle method.

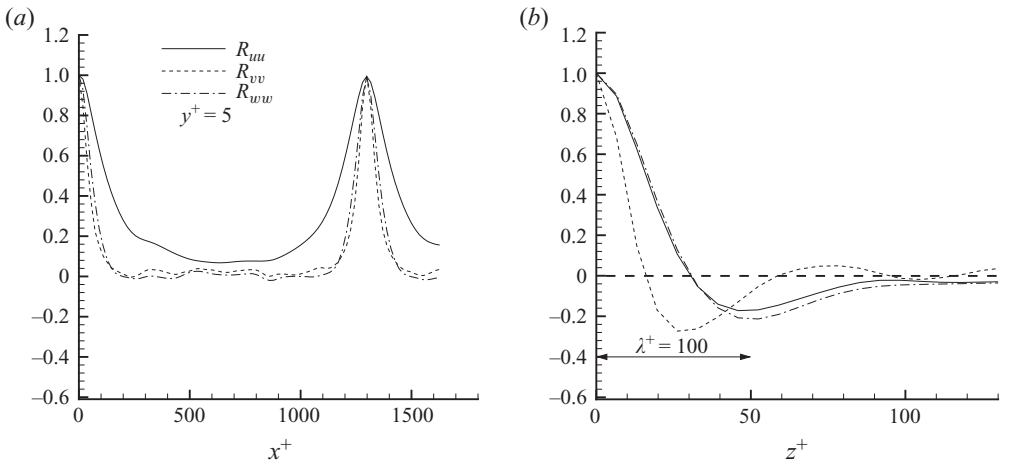

FIGURE 21. Two-point correlations for velocity fluctuations in ZPG at low Re_θ at $y^+ = 5$: (*a*) in the x-direction and (*b*) in the z-direction.

Finally, we remark that it will be of interest to generalize the new dynamic approach to capture the effects of roughness, compressibility, free-stream turbulence and curvature and to simulate the evolution of scalars.

This research was supported by the grants from the National Science Foundation (CBET 0829020) and the Office of Naval Research (Dr R. Joslin, programme manager). C.M. acknowledges support from Office of Naval Research project N00014-09-1-1007 at Johns Hopkins University (Dr R. Joslin, programme manager). Computational resources were supplied by TeraGrid (project no. TG-CTS090058) and Scientific Computation Research Center of the Rensselaer Polytechnic Institute. The authors thank Professor A. Ferrante from the University of Washington for providing his DNS data.

Appendix. Two-point correlations

To document the suitability of dimensions used for the computational domains, a two-point correlation analysis is performed along the streamwise and spanwise directions, for all velocity components. The two-point correlation function is defined as usual:

$$R_{u_i u_i}(x, y) = \frac{\overline{u_i'(0, y, z, t) u_i'(x, y, z, t)}}{u_i'(0, y)_{rms} u_i'(x, y)_{rms}}, \quad i = 1, 2, 3, \tag{A 1}$$

with no summation over i. Averaging is done over time t and over the spanwise position z in all cases. A similar expression is used for cross-stream spectra as a function of z, but additional averaging over x is performed.

Except for figure 21, all cases are for heights in the outer layer (figures 22–24) which is the most critical zone because of the presence of large-scale structures. In the cross-stream direction, displacements z for only half of the domain are shown because of the symmetry of the two-point correlations given by the periodic conditions. In the plots as a function of downstream distance, the peak at the recycle plane is expected,

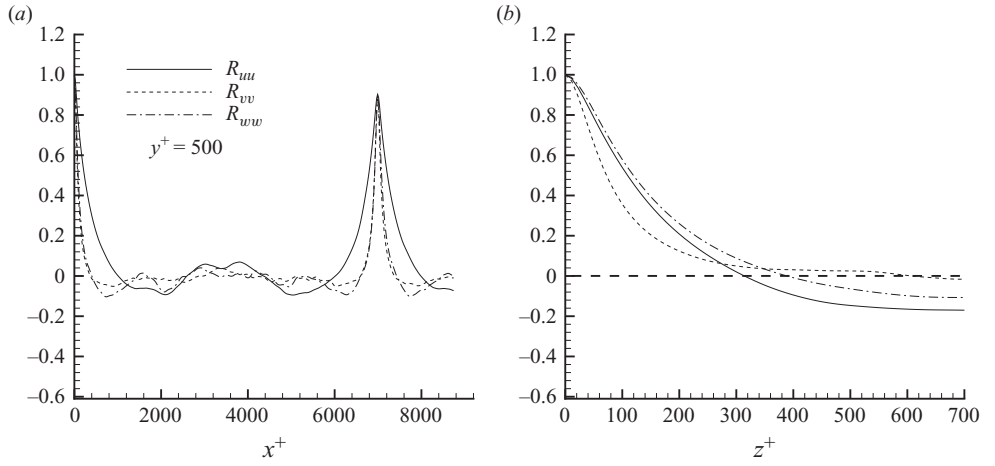

FIGURE 22. Two-point correlations for velocity fluctuations in ZPG at high Re_θ at $y^+ = 500$: (*a*) in the *x*-direction and (*b*) in the *z*-direction.

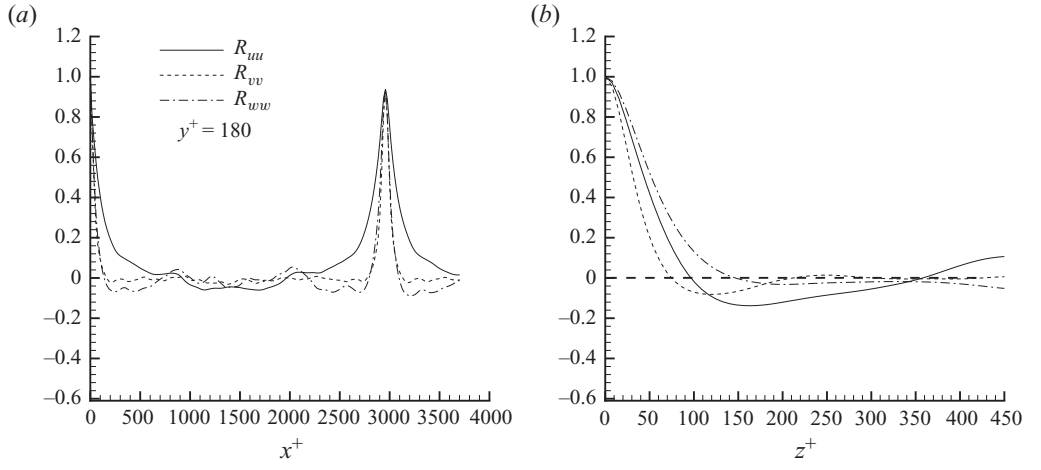

FIGURE 23. Two-point correlations for velocity fluctuations in an FPG flow at $y^+ = 180$: (*a*) in the *x*-direction and (*b*) in the *z*-direction.

since it is highly correlated with the inlet. In most cases, in the middle of the domain in both the streamwise and cross-stream directions, the correlations decay essentially to zero. As seen in figure 21, correlations in the near-wall regions decay quickly to zero. The same is true in all the other cases (not shown). In addition, correlations of u' in figure 21(*b*) exhibit a local minimum at $z^+ \approx 50$ for $y^+ = 5$, which indicates an average spacing ($\lambda^+ = \lambda u_\tau / \nu$) of low-speed streaks equal to 100. This is consistent with the generally accepted range of $\lambda^+ = 100 \pm 20$ in the near-wall region for canonical boundary layers (Smith & Metzler 1983; Kim & Moser 1987). In the outer regions, for some of the variables some residual correlations in the spanwise direction can be seen, especially in the APG case. Two-point correlations for the other test cases or locations (ZPG at low Re_θ in the outer region and FPG and APG closer to the wall) have shown decay to low correlation values, similar to the results shown in

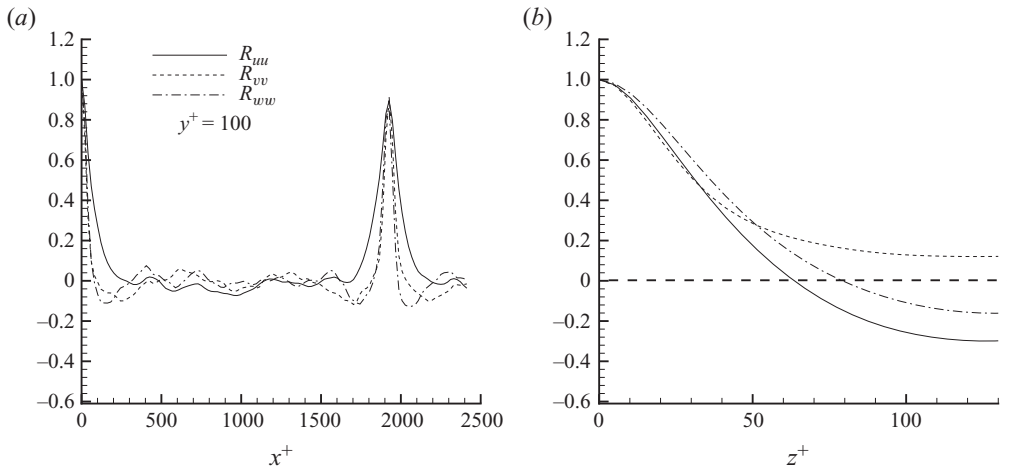

FIGURE 24. Two-point correlations for velocity fluctuations in a moderate-APG flow at $y^+ = 100$: (*a*) in the x-direction and (*b*) in z-direction.

figures 21–24. Still, wider and longer domains would obviously further decrease these correlations, but the domains are deemed appropriate for the goals of this study.

REFERENCES

ARAYA, G. 2008 DNS of turbulent wall bounded flows with a passive scalar. PhD thesis, Rensselaer Polytechnic Institute, Troy, NY.

ARAYA, G., JANSEN, K. & CASTILLO, L. 2009 Inlet condition generation for spatially-developing turbulent boundary layers via multi-scale similarity. *J. Turbul.* **10** (36), 1–33.

BALAKUMAR, B. J. & ADRIAN, R. 2007 Large- and very-large-scale motions in channel and boundary-layer flows. *Phil. Trans. R. Soc.* A **365**, 665–681.

CASTILLO, L. & GEORGE, W. K. 2001 Similarity analysis for turbulent boundary layer with pressure gradient: outer flow. *AIAA J.* **39** (1), 41–47.

DEGRAAFF, D. B. & EATON, J. K. 2000 Reynolds-number scaling of the flat-plate turbulent boundary layer. *J. Fluid Mech.* **422**, 319–346.

FERRANTE, A. & ELGHOBASHI, S. 2004 A robust method for generating inflow conditions for direct simulations of spatially-developing turbulent boundary layers. *J. Comput. Phys.* **198**, 372–387.

FERRANTE, A. & ELGHOBASHI, S. 2005 Reynolds number effect on drag reduction in a microbubble-laden spatially developing turbulent boundary layer. *J. Fluid Mech.* **543**, 93–106.

GEORGE, W. K. & CASTILLO, L. 1997 Zero-pressure-gradient turbulent boundary layer. *Appl. Mech. Rev.* **50**, 689–729.

GERMANO, M., PIOMELLI, U., MOIN, P. & CABOT, W. H. 1991 A dynamic subgrid-scale eddy viscosity model. *Phys. Fluids* A **3**, 1760–1765.

GUALA, M., HOMMEMA, S. E. & ADRIAN, R. 2006 Large-scale and very-large-scale motions in turbulent pipe flow *J. Fluid Mech.* **554**, 521–542.

HUTCHINS, N. & MARUSIC, I. 2007*a* Evidence of very long meandering structures in the logarithmic region of turbulent boundary layers. *J. Fluid Mech.* **579**, 1–28.

HUTCHINS, N. & MARUSIC, I. 2007*b* Large-scale influences in near-wall turbulence. *Phil. Trans. R. Soc.* A **365**, 647–664.

JANSEN, K. E. 1999 A stabilized finite element method for computing turbulence. *Comput. Meth. Appl. Mech. Engng* **174**, 299–317.

JONES, W. P. & LAUNDER, B. E. 1972 Some properties of sink-flow turbulent boundary layers. *J. Fluid Mech.* **56**, 337–351.

KAYS, W. M. & CRAWFORD, M. E., 1993 *Convective Heat and Mass Transfer*, 3rd edn. McGraw-Hill.

Keating, A., Piomelli, U., Balaras, E. & Kaltenbach, H. 2004 A priori and a posteriori tests of inflow conditions for large-eddy simulation. *Phys. Fluids* **16** (12), 4696–4712.

Kempf, A., Klein, M. & Janicka, J. 2005 Efficient generation of initial- and inflow-conditions for transient turbulent flows in arbitrary geometries. *Flow Turbul. Combust.* **74**, 67–84.

Khujadze, G. & Oberlack, M. 2004 DNS and scaling laws from new symmetry groups of ZPG turbulent boundary layer flow. *Theor. Comput. Fluid Dyn.* **18**, 391–411.

Kim, J. & Moser, R. 1987 Turbulence statistics in fully developed channel flow at low Reynolds number. *J. Fluid Mech.* **129**, 133–166.

Klein, M., Sadiki, A. & Janicka, J. 2002 A digital filter based generation of inflow data for spatially developing direct numerical or large eddy simulations. *J. Comput. Phys.* **186**, 652–665.

Kong, H., Choi, H. & Lee, J. 2000 Direct numerical simulation of turbulent thermal boundary layers. *Phys. Fluids* **12** (10), 2555–2568.

Le, H. & Moin, P. 1994 Direct numerical simulation of turbulent flow over a backward-facing step. *Rep.* TF-58. Thermosciences Division, Department of Mechanical Engineering, Stanford University.

Lee, J. & Sung, H. 2008 Effects of an adverse pressure gradient on a turbulent boundary layer. *Intl J. Heat Fluid Flow* **29** (3), 568–578.

Lee, S., Lele, S. & Moin, P. 1992 Simulation of spatially evolving turbulence and the applicability of Taylor's hypothesis in compressible flow. *Phys. Fluids* A **4**, 1521–1530.

Lund, T. S., Wu, X. & Squires, K. D. 1998 Generation of turbulent inflow data for spatially-developing boundary layer simulations. *J. Comput. Phys.* **140**, 233–258.

Mathis, R., Hutchins, N. & Marusic, I. 2009 Large-scale amplitude modulation of the small-scale structures in turbulent boundary layers. *J. Fluid Mech.* **628**, pp. 311–337.

Moin, P. & Mahesh, K. 1998 Direct numerical simulation: a tool in turbulence research. *Annu. Rev. Fluid Mech.* **30**, 539–578.

Na, Y. & Moin, P. 1998 The structure of wall-pressure fluctuations in turbulent boundary layers with adverse pressure gradient and separation. *J. Fluid Mech.* **377**, 347–373.

Osterlund, J. M. 1999 Experimental studies of zero pressure-gradient turbulent boundary-layer flow. PhD thesis, Royal Institute of Technology, Stockholm, Sweden.

Park, J. & Choi, H. 1999 Effects of uniform blowing or suction from a spanwise slot on a turbulent boundary layer flow. *Phys. Fluids* **11** (10), 3095–3105.

Perry, A. E., Marusic, I. & Jones, M. B. 2002 On the streamwise evolution of turbulent boundary layers in arbitrary pressure gradients. *J. Fluid Mech.* **461**, 61–91.

Rai, M. & Moin, P. 1993 Direct numerical simulation of transition and turbulence in a spatially evolving boundary layer. *J. Comput. Phys.* **109**, 169–192.

Schlatter, P., Orlu, R., Li, Q., Brethouwer, G., Fransson, J. H. M., Johansson, A. V., Alfredsson, P. H. & Henningson, D. S. 2009 Turbulent boundary layers up to $Re_\theta = 2500$ studied through simulation and experiment. *Phys. Fluids* **21** (5), 1070–6631.

Simens, M. P., Jimenez, J., Hoyas, S. & Mizuno, Y. 2009 A high-resolution code for turbulent boundary layers. *J. Comput. Phys.* **228** (11), 4218–4231.

Skote, M. 2001 Studies of turbulent boundary layer flow through direct numerical simulation. PhD thesis, Royal Institute of Technology, Stockholm, Sweden.

Smith, C. R. & Metzler, S. P. 1983 The characteristics of low-speed streaks in the near-wall region of a turbulent boundary layer. *J. Fluid Mech.* **129**, 27–54.

Smits, A. J., Matheson, N. & Jourbert, P. N. 1983 Low-Reynolds-number turbulent boundary layers in zero and favorable pressure gradients. *J. Ship Res.* **27** (3), 147–157.

Spalart, P. R. 1986 Numerical study of sink-flow boundary layers. *J. Fluid Mech.* **172**, 172–307.

Spalart, P. R. 1988 Direct simulation of a turbulent boundary layer up to $Re_\theta = 1410$. *J. Fluid Mech.* **187**, 61–98.

Spalart, P. R. & Leonard, A. 1985 Direct numerical simulation of equilibrium turbulent boundary layers. In *Proceedings of the 5th Symposium on Turbulent Shear Flows, Pennsylvania State University, University Park, PA* (ed. F. Durst, B. E. Launder, J. L. Lumley, F. W. Schmidt & J. H. Whitelaw), pp. 935–940. Springer.

Tejada-Martinez, A. E. & Jansen, K. E. 2005 On the interaction between dynamic model dissipation and numerical dissipation due to streamline upwind/Petrov–Galerkin stabilization. *Comput. Meth. Appl. Mech. Engng* **194**, 1225–1248.

Tejada-Martinez, A. E. & Jansen, K. E. 2006 A parameter-free dynamic subgrid-scale model for large-eddy simulation. *Comput. Meth. Appl. Mech. Engng* **195**, 2919–2938.

Trofima, A. V., Tejada-Martinez, A. E., Jansen, K. E. & Lahey, R. T. 2009 Direct numerical simulation of turbulent channel flows using a stabilized finite element method. *Comput. Fluids* **38**, 924–938.

White, F. M. 1974 *Viscous Fluid Flow*, 1st edn. McGraw-Hill.

Whiting, C. H. & Jansen, K. E. 2001 A stabilized finite element method for the incompressible Navier–Stokes equations using a hierarchical basis. *Intl J. Numer. Meth. Fluids* **35**, 93–116.

Wu, X. & Moin, P. 2009 Direct numerical simulation of turbulence in a nominally zero-pressure-gradient flat-plate boundary layer. *J. Fluid Mech.* **630**, 5–41.

Xu, S. & Martin, M. P. 2004 Assessment of inflow boundary conditions for compressible turbulent boundary layers. *Phys. Fluids* **16** (7), 2623–2639.